Three-dimensional presolidification heat transfer and fluid dynamics in molten microdroplet deposition ☆

V. Butty *, D. Poulikakos, J. Giannakouros

Laboratory of Thermodynamics in Emerging Technologies, Institute of Energy Technology, Swiss Federal Institute of Technology, ETH Center, Sonnegstrasse 3, 8092 Zurich, Switzerland

Abstract

The non-axisymmetric, coupled fluid mechanics and heat transfer of an impacting liquid solder droplet on a flat substrate is investigated numerically using the finite element method. The modelling of the fluid mechanics is based upon the full laminar Navier–Stokes equations employing a Lagrangian frame of reference. Due to the large droplet deformation, the surface (skin) as well as the volumetric mesh have to be regenerated during the calculations in order to maintain the high accuracy of the numerical scheme. The pressure and velocity fields are then interpolated on the newly created mesh. The energy equation is solved in both the droplet and the substrate domain. A time and space averaged thermal contact resistance is implemented between the two thermal domains (droplet and substrate). For the impact parameters used in this study (typical values $We = 2.38$, $Fr = 16,300$, $Re = 157$), the droplet rolls along the substrate but its shape remains practically axisymmetric for all the impact angles within the range from 0° to 60°. The substrate/droplet contact area is not a monotonically decreasing function of time and the cooling of the droplet is markedly dependent on the impact angle. © 2002 Published by Elsevier Science Inc.

Keywords: Free surface; Non-connected meshes; Droplet impact; Moving mesh; Lagrangian method

1. Introduction

The study of the interaction between a liquid droplet and a solid surface is of great relevance in many novel industrial applications, such as spray cooling, rapid prototyping, coating manufacturing and electronics manufacturing. The numerical investigation of these processes is important for the understanding of the underlying physics since it can give information, such as local temperature, velocity and pressure fields, which are not easily accessible experimentally due to the simultaneously small time and spatial scales, of the phenomena of interest. Most of the numerical studies undertaken so far are based on numerical methods like volume of fluid (VOF), arbitrary Lagrangian–Eulerian methods (ALE) and interface tracking, which target the Eulerian Navier–Stokes equations (Schunk et al., 2000; Oguz and Prosperetti, 1993). Unlike these methods, the numerical scheme employed in this study is based on the Lagrangian formulation of the Navier–Stokes equations. This is accomplished through an extension of the free surface-tracking scheme of Bach and Hassager (1985) into three dimensions.

The process considered in this study is related to solder jetting, where molten solder (63Sn37Pb) droplets with initial diameters D_0 impact on moving target substrates with an impact angle α and an impact velocity U_0. A schematic description of the three-dimensional droplet deposition problem is shown in Fig. 1a. After the droplet contacts the substrate, several scenarios may occur. First, a bounce-off of the droplet may occur after impact (Fig. 1b). Second, a rolling motion of the droplet on the surface along a distance from the point of impact may occur with subsequent solidification (Fig. 1c). Third, non-axisymmetric deformation and spreading around the locus of impact may occur (Fig. 1d). Since the droplet is simultaneously cooled by means of heat transfer to the substrate, it will eventually solidify, and ideally establish mechanical bonding to the substrate. A further fluid mechanical phenomenon that may occur

Nomenclature

I	identity matrix (–)
c_p	specific heat at constant pressure (J/kg K)
D	diameter (m)
$\vec{g}$	gravity (m/s^2)
k	thermal conductivity (W/mK)
p	pressure (Pa)
$\vec{m}$	binormal vector (–)
$\vec{n}$	normal direction (–)
q_n''	heat flux (W/m^2)
$R_{t,c}$	contact resistance (m^{2}K/W)
S	stress matrix (kg/m s^2)
$\vec{t}$	tangent direction (–)
u_{sound}	sound velocity (m/s)
u	velocity (m/s)

Dimensionless numbers

Pr	Prandtl $c_p\mu/k$
Re	Reynolds $\rho uD/\mu$
Pe	Peclet $Pr\,Re$

Greeks

μ	dynamic viscosity (kg/m s)
α_{ca}	contact angle (deg)
μ'	bulk viscosity (kg/m s)
θ	dimensionless temperature (–)
ε_{slip}	slip constant (–)
ε_{tol}	prescribed tolerance (–)
ξ, η	parametric coordinates
Ω	triangular element
γ	surface tension (N/m)
ρ	density (kg/m^3)
σ	stress tensor (N/m^2)

Superscript

0	initial value

Subscripts

l	parameter related to a liquid
s	parameter related to a solid

during the spreading phase of the droplet is breakup and splashing at high impact speeds. However, since our research is pertinent to jetting processes where such phenomena do not occur due to the small size of the drops, the high value of surface tension and the relatively low impact velocities, the efforts in this investigation are focused on the spreading and cooling of an impinging droplet, without splashing and breakup after impact. The bounce-off and rolling scenarios in Fig. 1b and c do not pose particular difficulties to our investigation. Three-dimensional convection is taken into account in the energy equation for the liquid and
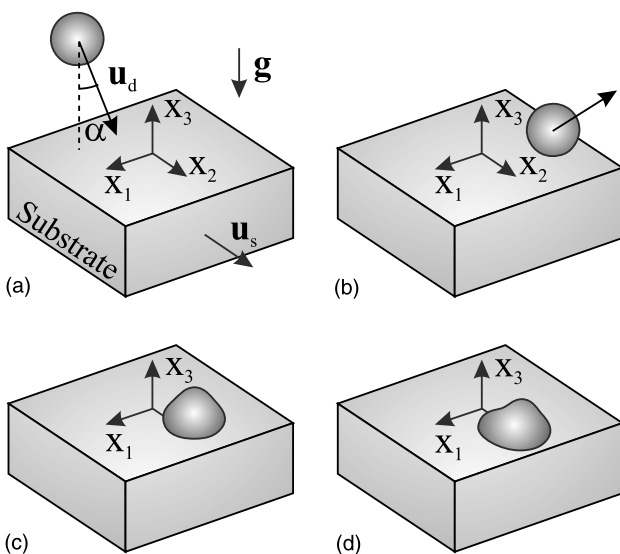

Fig. 1. Schematic description of the spreading. (a) In flight; (b) impact and bounce-off; (c) impact, rolling and spreading; (d) impact and spreading.
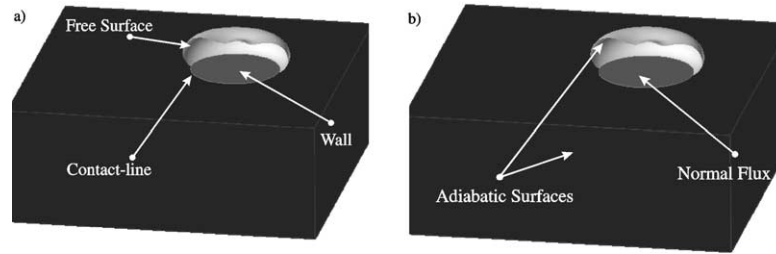
conduction in the substrate. Radiative heat transfer losses to the environment have been shown to be negligible compared to the heat transfer to the substrate (Waldvogel et al., 1996; Wallace et al., 1996; Waldvogel, 1995; Haferl et al., 2000). Hence, radiative losses are being neglected in our modelling. The model focuses on the presolidification regime. Solidification phenomena will be the topic of future work.

2. Formulation of the fluid mechanics model

The starting point of our theoretical investigation is the Lagrangian formulation of the Navier–Stokes equation (Eq. (1)). Although the fluid is assumed to be incompressible, this assumption is relaxed by applying the pseudo-compressibility scheme (Chorin, 1967; Baker and Carter, 1980). This approach is chosen in order to efficiently calculate the pressure field and circumvent the problems arising through the direct solution of the coupled Navier–Stokes and continuity equation

$$\begin{cases} \frac{1}{u_{sound}} \frac{\partial p}{\partial t} = -\rho \nabla \vec{u}, \\ \rho \frac{\partial \vec{u}}{\partial t} = \nabla \cdot S + \rho F, \end{cases}$$

$$S = \begin{pmatrix} 2\mu\frac{\partial u}{\partial x} - p & \mu\left(\frac{\partial u}{\partial y} + \frac{\partial v}{\partial x}\right) & \mu\left(\frac{\partial u}{\partial z} + \frac{\partial w}{\partial x}\right) \\ \mu\left(\frac{\partial u}{\partial y} + \frac{\partial v}{\partial x}\right) & 2\mu\frac{\partial u}{\partial x} - p & \mu\left(\frac{\partial v}{\partial z} + \frac{\partial w}{\partial y}\right) \\ \mu\left(\frac{\partial u}{\partial z} + \frac{\partial w}{\partial x}\right) & \mu\left(\frac{\partial v}{\partial z} + \frac{\partial w}{\partial y}\right) & 2\mu\frac{\partial u}{\partial x} - p \end{pmatrix}$$

$$+ \mu'\left(\frac{\partial u}{\partial x} + \frac{\partial v}{\partial y} + \frac{\partial w}{\partial z}\right)I. \tag{1}$$

Fig. 2. Fluid and thermal boundary conditions.

The bulk viscosity μ' appearing in the stress matrix S is set according to the literature to 1/3 of the dynamic viscosity μ (Ryhming, 1985). It is also assumed that the only body force acting on the fluid is gravity.

2.1. Boundary conditions

2.1.1. Substrate surface

At the contact interface between the droplet and the substrate, except in a small region near the contact-line (CL), the conventional no-slip boundary condition is being applied (Fig. 2a)

$$\vec{u}_l = \vec{u}_w. \tag{2}$$

2.1.2. Navier slip model

In the vicinity of the CL, the fluid is allowed to slip on the substrate according to the Navier slip hypothesis (Eq. (3)) in order to circumvent unbounded stresses at the CL (Dussan and Davis, 1974) (Fig. 2a)

$$\vec{n} \cdot S \cdot \vec{t} = \frac{1}{\varepsilon_{\text{slip}}} (\vec{u}_l - \vec{u}_w) \cdot \vec{t}. \tag{3}$$

In Eq. (3), $\vec{n}$ stands for the normal vector to the surface and $\vec{t}$ for the tangent vector. $\vec{u}_w$ is the velocity of the substrate and $\varepsilon_{\text{slip}}$ is a slip coefficient.

2.1.3. Free surface

At the free surface of the droplet, the boundary condition is given by the Laplace equation (Eq. (4)), which balances the viscous stresses on both sides of the interface with the pressure term arising through the surface tension (Landau and Lifshitz, 1959) (Fig. 2a)

$$\vec{n} \cdot \left(S^{(2)} - S^{(1)} \right) - \nabla_s \sigma = -\sigma(\nabla_s \cdot \vec{n})\vec{n}. \tag{4}$$

In Eq. (4), σ is the surface tension coefficient, ∇_s is the surface gradient operator and $\vec{n}$ is the outward normal unit vector. The assumption is made that the interaction with the surrounding gas at constant pressure p_1 with the free surface can be neglected during the impact process. Hence, $\vec{n} \cdot S^{(1)} = 0$. In the finite element implementation, the boundary condition at the free surface takes the following form:

$$\int S \cdot \vec{n}\,dS = \int \frac{1}{We} (\nabla_s \varphi_i)\,dS - \oint \frac{1}{We} \varphi_i \vec{m}\,dC, \tag{5}$$

where, $\vec{m}$ is the unit outward surface tangent vector normal to the curve and φ_i are the finite element basis functions. The definition of $\vec{m}$ does not force the contact angle to have a specific value. It merely imposes a net interfacial force at the CL (Bach and Hassager, 1985). The unit outward surface tangent vector, $\vec{m}$, is defined to be orthogonal to the unit substrate normal $\vec{n}$ (Fig. 3). Hence, the current modelling of the CL region corresponds to a non-wetting fluid motion on the substrate. However, the extension to a wetting fluid motion (e.g. variable contact angle α_{ca}) would not pose serious problems provided that additional experimental information were available (i.e. the spatial distribution of the dynamic contact angle). In this case, one can define $\vec{m}$ through the following geometrical relationship $\vec{m} = \vec{n}\cos(\alpha_{\text{ca}}) - \vec{b}\sin(\alpha_{\text{ca}})$, in which $\vec{b}$ is defined as

$$\vec{b} = \frac{\vec{n} \times \vec{t}}{|\vec{n} \times \vec{t}|}.$$

2.1.4. Initial conditions

The initial velocity field in the droplet is uniform and set to the non-dimensionalized initial droplet velocity. Since the initial shape of the droplet is a sphere, the pressure distribution is uniform so that the droplet is in an equilibrium state

$$\vec{u}_0 = \frac{\vec{U}_0}{\|\vec{U}_0\|}, \quad p = \frac{4}{We}.$$
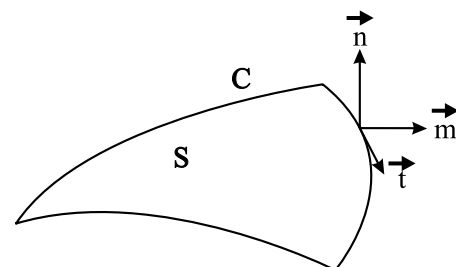
Fig. 3. Definition of the vector $\vec{m}$.

The deformation of the droplet mesh is calculated using the free surface-capturing scheme proposed by Bach and Hassager (1985). Since the accuracy of the finite element results strongly depends on the volumetric and surface mesh quality, the generation of a new droplet mesh is needed when the mesh elements do not fulfill certain quality criteria (Eq. (6)). In cases where the surface mesh has to be re-generated, the surface is reconstructed with a NURBS surface upon which the new surface mesh is generated. The pressure and velocity fields are then interpolated on the new mesh

$$D_e = \frac{\sum_n J_n W_n}{\min_n |J_n W_n| N} \geq \varepsilon_{\text{tol}}. \tag{6}$$

In Eq. (6), n is the number of integration points and W_n their weight factor. J_n is the determinant of the finite element mapping at the integration point. In the case of a higher order finite element, D_e is the ratio between the volume of the element transformed by the finite element mapping versus the minimum discreet mapped volume. This function reaches the minimum $D_e = \sum_n W_n / \min_n |W_n| N$ and tends to infinity as the element deforms. In our case, we set the limit value ε_{tol} to this function to a constant of the order of 2.

3. Heat transfer

Due to the employment of a Lagrangian frame of reference, the energy equations for both the droplet as well as the substrate have the same form, Eq. (7). Dissipation effects in the energy equation are neglected. The substrate is assumed to be isotropic concerning its thermal conductivity and its specific heat

$$Pe \frac{\partial \Theta}{\partial t} = \Delta \Theta, \quad \Theta = \frac{T - \min(T_l^0, T_s^0)}{|T_l^0 - T_s^0|}. \tag{7}$$

The Galerkin finite element method belongs to the numerical methods based on a space integration of the weighted underlying equation, called the weak formulation. The variables of interest are interpolated within the physical domain with compact support functions and the weighting functions are defined in this particular method as a linear combination of interpolation basis functions (Gunzburger, 1989; Zienkiewicz, 1997; Gresho et al., 1999). Hence, the Galerkin weak formulation of the non-dimensionalized equation (Eq. (7)) is written as:

$$Pe \sum_{j=1}^{m_t} \frac{\partial \theta_j}{\partial t} \sum_{i=1}^{m_t} \int_{\Omega_e} \psi_i \psi_j \, \mathrm{d}V + \sum_{j=1}^{m_t} \theta_j \sum_{i=1}^{m_t} \int_{\Omega_e} \left(\frac{\partial \psi_i}{\partial x} \frac{\partial \psi_j}{\partial x} \right.$$
$$\left. + \frac{\partial \psi_i}{\partial y} \frac{\partial \psi_j}{\partial y} + \frac{\partial \psi_i}{\partial z} \frac{\partial \psi_j}{\partial z} \right) \mathrm{d}V = L, \tag{8}$$

where the term L is defined as:

$$L = \int_{\Omega_e} k \psi_i n \cdot \nabla \theta \, \mathrm{d}S. \tag{9}$$

The boundary conditions linked to the heat transfer are of two kinds. The first one is an adiabatic boundary condition (Fig. 2b), which is set on every surface of the domain except at the interface between the droplet and the substrate. Former studies have shown that for in this range of temperatures the heat removal from the droplet is overwhelmingly driven through the conduction between the droplet and the substrate (Wallace et al., 1996; Waldvogel, 1995; Poulikakos and Waldvogel, 1997). Hence, we neglect radiation or convective losses to the environment. The second boundary condition is an applied heat flux (Fig. 2b), at the interface of the droplet and the substrate, in order to accommodate the effect of thermal resistance. The heat flux at this location is determined using Eq. (10), in which $R_{t,c}$ is the thermal contact resistance between the liquid and the substrate

$$q_n'' = \frac{\theta_l - \theta_s}{R_{t,c}}. \tag{10}$$

The contact resistance stems from the fact that during the spreading of the liquid on the substrate and in particular after freezing (nor modelled in the present investigation) a perfect contact between the liquid and solid cannot be achieved, due to possible surface roughness, surface tension of the melt and impurities on the surface.

The solidified droplet shape depends on the impact conditions but also on the cooling rate of the liquid phase (Attinger et al., 2000). The contact resistance influences this cooling rate. Waldvogel, 1995 uses a special layer of finite elements between the liquid phase and the solid phase allowing only for conduction normal to the surface. The height of this layer was determined as a function of the contact resistance. Using a mesh adaptive algorithm and tuning the value of the contact resistance, they achieved good agreement between experimental and numerical results. Nevertheless, this approach seemed quite inappropriate for an implementation in a three-dimensional code regarding on the one hand the operations implied by the mesh adaptation algorithm and on the other hand the element quality within this layer. The mesh adaptation algorithm implies that for each droplet node reaching the substrate at a certain location, a node belonging to the substrate mesh must also be moved to this location. This operation implies the adaptation of the temperature of the moved substrate node at its new position. In a three-dimensional code, this would lead to a marked time requirement in comparison to the time needed to solve the heat transfer equation. Moreover, the elements within the thermal resistance layer would sense two length scales; the first one related to the mesh size parallel to the

substrate surface and the second related to the mesh height of the thermal contact resistance layer. The relation between the two length scales would lead to elements with high aspect ratios, which are known to decrease the solution accuracy. Hence, we implemented the following improved iterative process for the conjugate heat transfer, based on the approximation of the active flux between the solid and liquid phase.

The determination of L in Eq. (11) implies the integration of the flux over an element. In order to perform the numerical integration, we interpolate the heat flux within the element using the finite element basis function (Zienkiewicz, 1997). Therefore, the heat flux is calculated at each nodal point of the droplet–substrate interface elements. To this end, at the interface, the boundary term is defined as:

$$L = -\sum_{j=1}^{m_t} q''_{n,j} \int \psi_i \psi_j \, \mathrm{d}S. \tag{11}$$

In order to calculate the flux at each nodal point, the corresponding temperature on the adjacent mesh must be found. This operation involves the following steps:

- The projection of the node onto the non-connected/adjacent surface mesh is carried out and, if the distance between the node and its projection is less than a fixed tolerance, the node is taken into account in the heat flux evaluation process (Fig. 4).
- For each and every selected node, the corresponding temperature on the adjacent surface mesh is interpolated using its projection.

The projection of a node is evaluated using Eq. (12) based upon the fact that the surface of the adjacent mesh is defined as a collection of parametric surface patches given through the finite element mapping. In Eq. (12), P is the node under consideration, S is the surface of a finite element and (ξ, η) are the parametric coordinate of the point within the element. In the case of a triangular element the relationships $0 \leqslant (\xi, \eta, 1 - \xi - \eta) \leqslant 1$ must hold
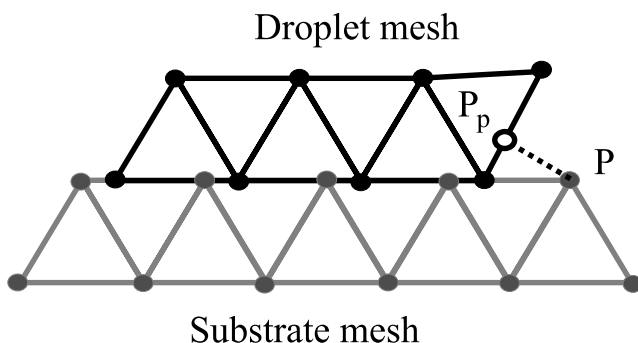

Droplet mesh

Substrate mesh

Fig. 4. Projection of a node on the adjacent mesh.

$$\begin{cases} (\vec{S}(\xi,\eta) - \vec{P}) \cdot \vec{S}_\varepsilon(\xi,\eta) = 0 \\ (\vec{S}(\xi,\eta) - \vec{P}) \cdot \vec{S}_\eta(\xi,\eta) = 0 \end{cases},$$

$$\vec{S}(\xi,\eta) = \sum_{i=1}^{n} \varphi_i(\xi,\eta)\vec{x}_i. \tag{12}$$

Since the droplet and substrate meshes are not connected (Fig. 4), the fluxes calculated from the droplet to the substrate and vice versa differ slightly due to the variation of the numerical definition of the interface surface. In order to take into account this variation in heat transfer, a geometrical correction factor β is introduced in the flux term:

$$\beta = \frac{E_1}{E_s}, \quad E_i = \sum_{n=1}^{m} \int_{\Omega_{n,j}} q'' \, \mathrm{d}S, \tag{13}$$

where, E_1 and E_s are the respective energies transferred from the droplet and to the substrate. The corrected flux term can be written as:

$$L = -\beta \sum_{j=1}^{m_t} q''_{n,j} \int \psi_i \psi_j \, \mathrm{d}S. \tag{14}$$

During the calculation of β, the energy transferred from the droplet to the substrate is defined as the energy of reference. Thus, while calculating the flux term for the droplet, β is set to 1.

Within a thermal time step, an iterative process is performed in order to calculate the temperature distribution within the droplet and the substrate. At each sub-iteration n a new flux is calculated using the temperature distribution T^n, which leads to a new temperature distribution T^{n+1}. This process is performed until the temperature at each nodal point has converged. The iterative process convergence criterion is defined as:

$$\frac{T^{n+1} - T^n}{T^n - T^0} \leqslant \varepsilon_{\text{tol}} \tag{15}$$

in which, ε_{tol} is a prescribed tolerance O(10^{-3}).

3.1. Initial condition

The initial conditions for the heat transfer are in non-dimensional form read:

$$\theta_1 = 1, \quad \theta_s = 0.$$

4. Results

The following results refer to the impact (prior to freezing) of a liquid solder droplet on a flat aluminium substrate. The contact resistance between the droplet and the substrate is $R_{t,c} = 1 \times 10^{-6}$, corresponding to a value of the interface heat transfer coefficient of 1×10^6, a high value corresponding to very good thermal con-
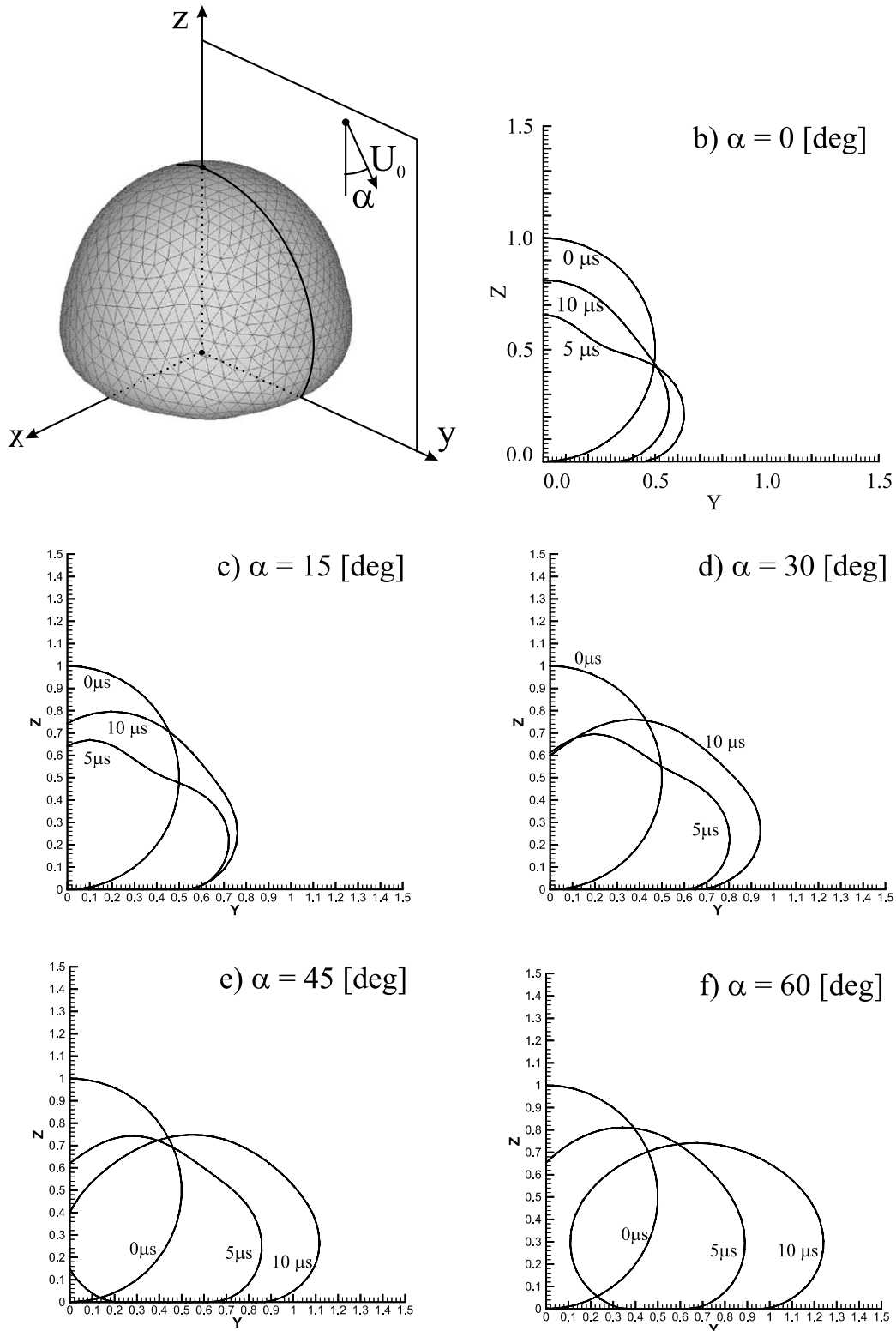
Fig. 5. Sequence of droplet profiles for equal impact conditions but different impact angles.

tact. This is indeed the case in the present study focusing on the pre-solidification regime. The initial temperature of the droplet and the substrate are respectively 350 and 200 °C. The impact velocity is 2 m/s and the initial droplet diameter is 25×10^{-6} m. The impact angle with respect to the normal to the substrate ranges from 0° to
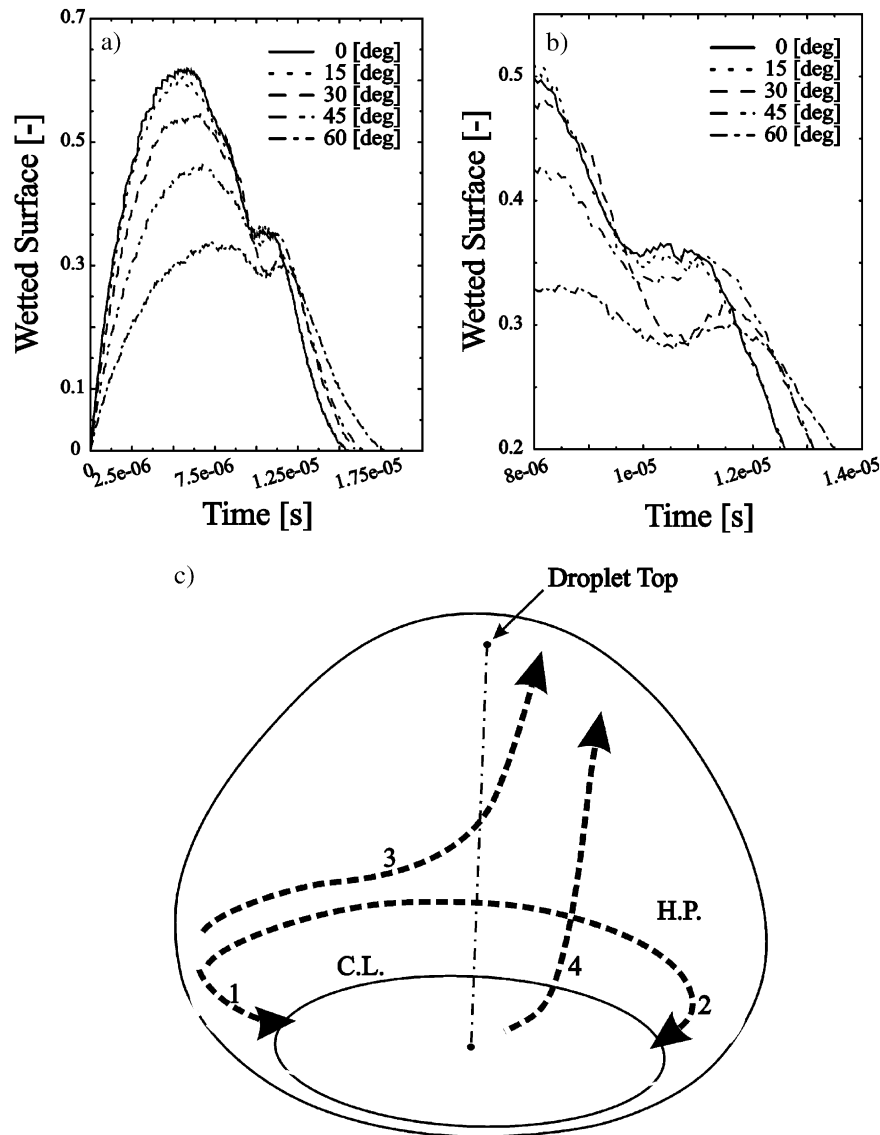
Fig. 6. Evolution of the contact area for various impact angles.

60°. Hence, the characteristic non-dimensional numbers describing the fluid motion are $We = 2.38$, $Fr = 16,300$, $Re = 157$. The initial velocity vector in the droplet domain has the following form $(v_x, v_y, v_z) = U_0(0, -\cos \alpha, \sin \alpha)$. The substrate is stationary. Regarding the finite element discretization, the velocity field is calculated using second order tetrahedral elements, the pressure and the temperature are calculated on linear tetrahedral elements. A typical mesh for the droplet domain consists of approximately 15,000 elements and 45,000 elements for the substrate mesh respectively.

4.1. Fluid mechanics

Calculations of the droplet deposition using various impact angles show that the droplet deforms and rolls during impact. The three dimensionality of the process is induced primarily by the rolling process (more significant at larger impact angles). The cross-section of the droplet in the y–z-plane remains practically axisymmetric (Fig. 5). These results makes sense physically due to the preponderant role played by the surface tension (high for liquid metals such as solder) during the impact, and the fact that the substrate is modelled to be ideally smooth and not wetted by the droplet material.

For equal impact conditions (e.g. equal Re, We and Fr) but increasing impact angles, the droplet deforms less and rolls more due to the decreasing normal velocity component at impact. The two limit cases are defined as the normal impact, which leads to an axisymmetric deformation and the parallel rolling of the droplet on the substrate. In Fig. 5 slices of the droplet mesh are pre-
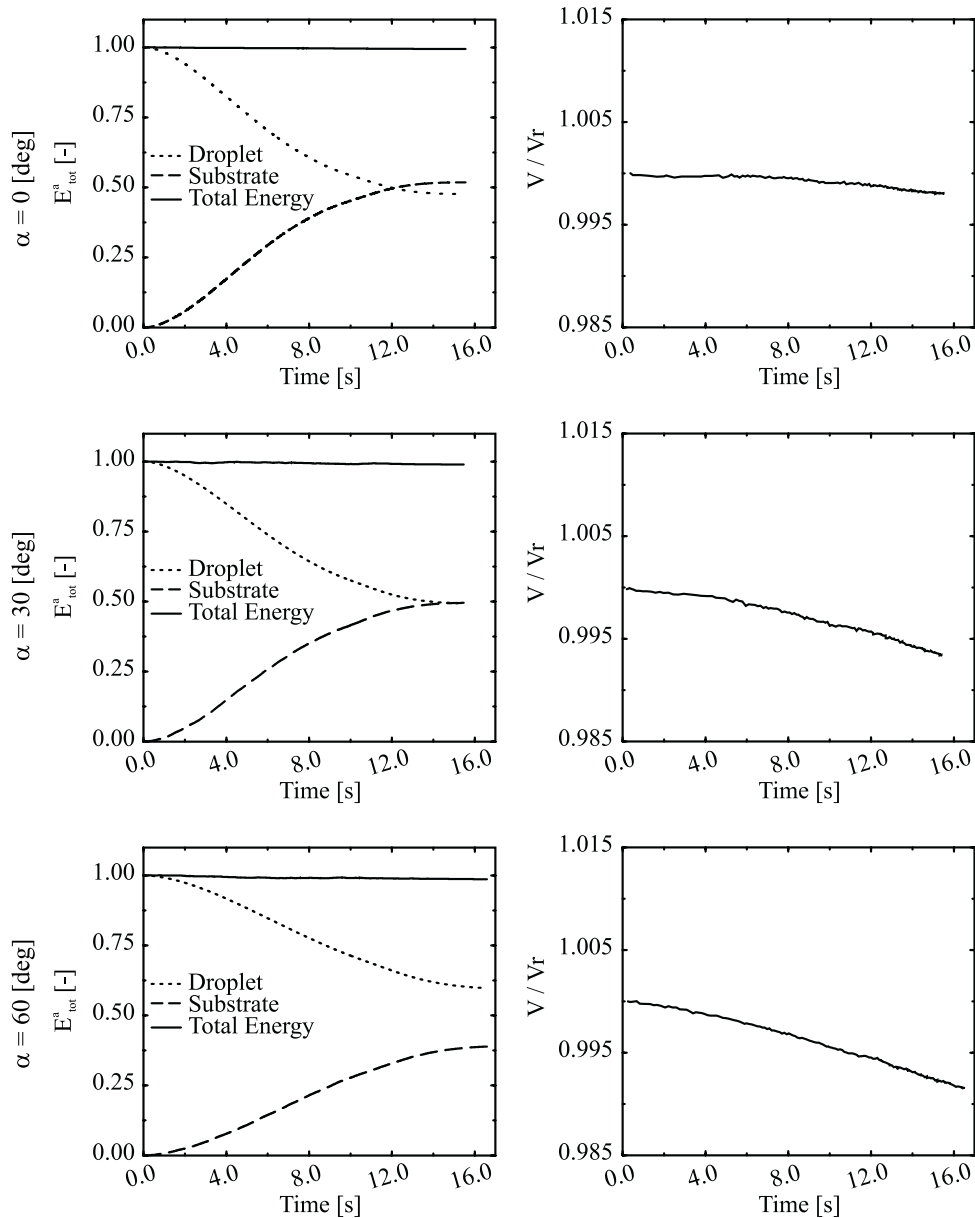
Fig. 7. Energy conservation, droplet volume and energy fluctuation for various impact angles.

sented along the plane containing the initial velocity vector of the droplet and the normal to the substrate at the initial impact point (Fig. 5a). In Fig. 5b–f, the increasing sliding/rolling motion of the droplet with an increasing impact angle can be clearly observed. This is due to the increasing tangential velocity component of the droplet to the substrate. Apparent is also the diminishing overall deformation of the droplet with an increasing impact angle.

An important aspect for any droplet/surface interaction heat transfer process is the contact surface area. In the solder jetting process the contact surface area, directly affects the cooling of the droplet and therefore the solidified footprint, the size of which affects the

mechanical bonding of the deposited material on the substrate. In Fig. 6a the contact area between the droplet and the substrate is shown for various impact angles. The behavior of the temporal evolution of the contact surface can be divided into four regimes. The first regime corresponds to the spreading of the droplet followed by the second regime, which is the first stage of receding/recoiling period. During the recoiling regime (contact area decreasing with time) there is a small intermittent regime of local spreading which can be explained by the appearance of high pressure zones (HP) in the fluid close to the substrate surface (Fig. 6c). This zone close to the substrate prohibits the fluid near the substrate to move into the upward direction. It separates
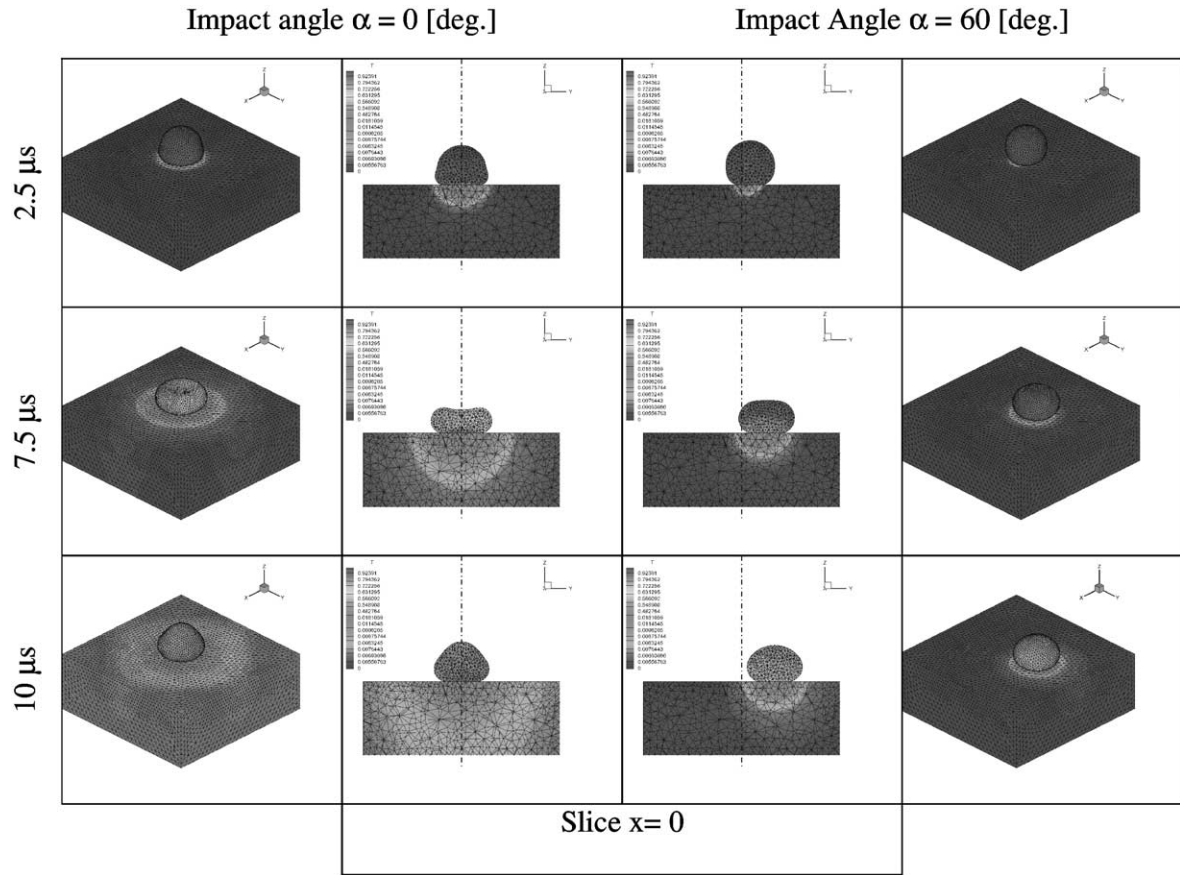
Fig. 8. Temperature distribution within the droplet and the substrate.

the fluid flow near the free surface in an upward flow (3) and a downward flow (1) and (2). The downward flow will contribute to a local increase of the curvature of the droplet surface near the CL. The high pressures generated in this zone will force part of the surface to re-attach to the substrate, hence increase the contact surface again. This will temporally halt the receding motion and convert it into a spreading motion. In summary, the existence of this third regime is due to the disparity of time scales between the fluid dynamics inside the droplet and the surface tension driven recoiling process.

During the remainder of the receding (fourth regime), the contact surface decreases with time. It also increases with the impact angle. This latter behaviour is due to the fact that the normal to the substrate kinetic energy of the droplet is reduced with increasing impact angle, which in turn results in a reduction of the surface potential energy at the end of the spreading and in less subsequent recoiling driven by this potential energy.

4.2. Heat transfer

Due to the time and length scales of the physical phenomena under investigation, it is very difficult to acquire experimental information regarding the local temperature distribution in the droplet and the substrate. Therefore, we will validate the accuracy of the heat transfer model by considering conservation of the total thermal energy E_{tot} of the droplet/substrate system. The dimensionless total thermal energy E_{tot}^a is defined as:

$$E_{tot}^a = \frac{\int_{V_d} \rho c_{p,d}(T - \min(T_d^0, T_s^0))\,dV + \int_{V_s} \rho c_{p,s}(T - \min(T_d^0, T_s^0))\,dV}{\int_{V_d} \rho c_{p,d}(T_d^0 - \min(T_d^0, T_s^0))\,dV + \int_{V_s} \rho c_{p,s}(T_s^0 - \min(T_d^0, T_s^0))\,dV}.$$

In typical calculations, where 1500 iterations correspond to approximately 15 μs of real time, a loss or gain in thermal energy of only up to 1.5% can be observed as shown in Fig. 7. A reason for this clearly acceptably small error (taking into account the complexity of the simulations), is that during remeshing operations a surface fitting algorithm based on NURBS is applied to describe the free surface of the impacting droplet, as already mentioned above. This operation can lead to small changes of the droplet volume (the excellent overall volume conservation performance of the numerical code is also shown in Fig. 7). Since the definition of the surface is slightly changed through the fitting algorithm, small errors in the interpolation of the temperature, velocity and pressure fields occur. These fluctuations in the above mentioned variable fields, which

are on the order of 0.05% for each remeshing operation, lead to fluctuations in the total thermal energy. Third, in the evaluation of the heat flux between the droplet and the substrate small errors in the calculation of the affected, active heat transfer area can lead to additive errors in the total thermal energy. In other words, since the calculated energy exchanged by heat transfer during each time-step is based on a calculated local heat flux multiplied by a fractional surface, errors in the evaluation of the active heat transfer surface can lead to differences in the energy transferred out of the droplet domain and the energy transferred into the substrate domain. This error contributes to the total thermal energy loss or gain after many iterations. With the above assessment in mind one must appreciate the fact that energy in indeed well conserved in the present calculations.

A comparison of Fig. 7 as well as the temporal temperature field information of Fig. 8 show clearly that the heat removal from the droplet is deduced markedly with increasing impact angle (measured away from the normal to the substrate). This is due to the fact that the contact area is reduced with increased impact angle. In addition, the convective effect in the droplet is reduced with increasing impact angle, since the droplet follows more of a rolling motion with reduced impact-induced internal flow velocities, in particular in the vertical direction.

5. Conclusions

The study concluded that the three-dimensional behavior of the droplet impact is primarily captured through a rolling/translational motion, more noticeable at high impact angles with respect to the normal to the surface. We have shown that for the current impact parameters of interest, the droplet rolls but remains practically axisymmetric during the impact regardless of the large values (up to 60°) of impact angle considered. The surface tension has a correcting effect and promotes axisymmetry. Neither splashing phenomena nor fingering formation was observed within the parametric domain of this work.

The heat transfer problem was solved using a method based on two non-connected meshes. Despite inherent small total thermal energy losses, this method has been implemented with success. Total thermal energy losses for an entire calculation cycle were less than 1.5% in all cases, which is within acceptable tolerance in regard to the complexity of the problem under consideration.

We also demonstrated that during the recoiling of the droplet, the contact area does not decrease monotonically. Finally, the cooling of the droplet is markedly dependent on the impact angle.

References

Attinger, D., Haferl, S., Zhao, Z., Poulikakos, D., 2000. Transport phenomena in the impact of a molten droplet on a surface: macroscopic phenomenology and microscopic considerations. Part II: Heat transfer and solidification. Reviews in Heat Transfer, Vol. XI. Begell House, New Yok, pp. 145–205.

Bach, P., Hassager, O., 1985. An algorithm for the use of the lagrangian specification in newtonian fluid mechanics and applications to free-surface flow. J. Fluid Mech. 152, 173–190.

Baker, A.J., Carter, F.D., 1980. Accuracy and stability of a finite element pseudo-compressibility CFD algorithm for incompressible thermal flow. Numer. Heat transfer. Part B 20, 1–23.

Chorin, A.J., 1967. A numerical method for solving incompressible viscous flow. J. Comput. Phys. 2, 12–26.

Poulikakos, D., Waldvogel, J., 1997. Solidification phenomena in picoliter size solder droplet deposition on a composite substrate. Int. J. Heat Transfer 40 (2), 295–309.

Dussan, E.B., Davis, S.H., 1974. On the motion of a fluid–fluid interface along a solid surface. J. Fluid Mech. 65, 71–95.

Gresho, P.M., Engelman, M.S., et al., 1999. Incompressible Flow and Finite Element Method: Advection–Diffusion and Isothermal Flow. John Wiley and Sons, Chichester.

Gunzburger, M.D., 1989. Finite Element Methods for Incompressible Flows: a Guide to Theory, Practice and Algorithm. Academic Press Inc., San Diego.

Haferl, S., Zhao, Z., Giannakouros, J., Attinger, D., Poulikakos, D., 2000. Transport phenomena in the impact of a molten droplet on a surface: macroscopic phenomenology and microscopic considerations. Part I: Fluid dynamics. Reviews in Heat Transfer, Vol. XI. Begell House, New Yok, pp. 65–143.

Landau, L.D., Lifshitz, E.M., 1959. Fluid Mechanics, Course of Theoretical Physics. 6.

Oguz, H.N., Prosperetti, A., 1993. The impact of drops on liquid surfaces and the underwater noise of rain. Ann. Rev. Fluid Mech. 25, 577–602.

Ryhming, I., 1985. Dynamique des fluides, deuxième édition. Lausanne, Presses Polytechniques et Universitaires Romandes.

Schunk, P.R., Rao, R.R., et al., 2000. A finite element method for free-surface flows of incompressible fluids in three dimensions. Part II: dynamic wetting lines. Int. J. Numer. Meth. Fluids 33, 405–427.

Waldvogel, J.M. 1995. Transport Phenomena and Solidification in Picoliter Solder Droplet Deposition, University of Illinois at Chicago.

Waldvogel, J.M., Poulikakos, D., et al., 1996. Transport phenomena in picoliter size solder droplet dispension on composite substrate. J. Heat Transfer 118, 148–156.

Wallace, D.B., Waldvogel, J.M., et al., 1996. Transport phenomena in picoliter size solder droplet dispension on a composite substrate. J. Heat Transfer 118, 148–156.

Zienkiewicz, O.C., 1997. The Finite Element Method, vol. 1, fourth ed. McGraw Hill, London.